Coupled-mode theory for spatial gap solitons in optically induced lattices

Boris A. Malomed
Department of Interdisciplinary Studies, School of Electrical Engineering, Faculty of Engineering, Tel Aviv University, Tel Aviv 69978, Israel

Thawatchai Mayteevarunyoo
Department of Telecommunication Engineering, Mahanakorn University of Technology, Bangkok 10530, Thailand

Elena A. Ostrovskaya and Yuri S. Kivshar
Nonlinear Physics Center, Research School of Physical Sciences and Engineering, Australian National University, Canberra ACT 0200, Australia

(Received 24 December 2004; published 26 May 2005)

We derive two systems of coupled-mode equations for spatial gap solitons in one-dimensional (1D) and quasi-one-dimensional (Q1D) photonic lattices induced by two interfering optical beams in a nonlinear photorefractive crystal. The models differ from the ordinary coupled-mode system (e.g., for the fiber Bragg grating) by saturable nonlinearity and, if expanded to cubic terms, by the presence of four-wave-mixing terms. In the 1D system, solutions for stationary gap solitons are obtained in an implicit analytical form. For the Q1D model and for tilted ("moving") solitons in both models, solutions are found in a numerical form. The existence of stable tilted solitons in the full underlying model of the photonic lattice in the photorefractive medium is also shown. The stability of gap solitons is systematically investigated in direct simulations, revealing a nontrivial border of instability against oscillatory perturbations. In the Q1D model, *two disjointed* stability regions are found. The stability border of tilted solitons does not depend on the tilt. Interactions between stable tilted solitons are investigated too. The collisions are, chiefly, elastic, but they may be inelastic close to the instability border.

DOI: 10.1103/PhysRevE.71.056616 PACS number(s): 05.45.Yv, 42.65.Tg, 42.70.Nq

I. INTRODUCTION

It is well known that a periodic modulation of the optical refractive index not only modifies the spectrum of linear waves, but also strongly affects the nonlinear propagation and self-trapping of light [1,2]. Recently, the formation of spatial solitons in optically induced reconfigurable photonic lattices created in photorefractive materials was predicted in Ref. [3] and demonstrated experimentally in one-dimensional (1D) [4,5] and two-dimensional (2D) [6] geometries. In this case, the strong electro-optic anisotropy of a photorefractive crystal is employed to create the lattice by two (or more) interfering laser beams in the ordinary polarization, while the solitons are observed in the probe beam, which is launched in a strongly nonlinear mode with the extraordinary polarization.

Periodically modulated nonlinear systems can also support self-trapped localized pulses or beams in the form of *gap solitons* (GS's), which are hosted by a band gap of the system's linear spectrum, induced by the resonant Bragg coupling between forward- and backward-propagating waves [2,7]. A notable property of the GS's is that, unlike ordinary solitons which require self-focusing nonlinearity, they can exist in both self-focusing and self-defocusing media.

Traveling temporal-domain GS's have been observed experimentally in Bragg gratings written in silica fibers [8]. The concept of a spatial-domain GS was also proposed [9,10] and elaborated in more detail [11–13] in various waveguide settings. Experimentally, spatial GS's were created in waveguide arrays [14] and optically induced photonic lattices [15], using a two-beam excitation scheme.

A generic description of the GS's is provided by the coupled-mode theory (CMT), which amounts to the derivation of a system of coupled equations for interaction of forward and backward waves [7]. The standard CMT system for media with Kerr (cubic) nonlinearity is equivalent to a generalized massive Thirring model. However, unlike the massive Thirring model proper that includes only cross-phase-modulation (XPM) nonlinear terms, its generalized version [which includes self-phase-modulation (SPM) too] is not integrable. Nevertheless, a family of its GS solutions can be found in an explicit analytical form [16]. These solutions depend on two essential parameters, which determine the soliton's amplitude and velocity. The stability of the GS's was first investigated by means of the variational approximation in Ref. [17] and then, with the help of rigorous methods, based on numerical computation of stability eigenvalues [18]. Both approaches demonstrate that the GS family has a nontrivial border of stability against oscillatory perturbations, while the entire family is stable against nonoscillatory perturbations in accordance with the Vakhitov-Kolokolov (VK) criterion [19] applied to these solitons.

In this paper, we study soliton effects in photonic lattices induced by interfering optical beams in a nonlinear photorefractive crystal and derive two CMT models for spatial GS's, which correspond to the 1D and quasi-1D (Q1D) geometries. Unlike the usual generalized massive Thirring model, these models feature saturable nonlinearity and, if expanded to cubic terms order, the proper-1D model includes not only XPM

and SPM terms, but also four-wave mixing (FWM) and nonlinear-coupling ones.

The paper is organized as follows. In Sec. II we consider, in a brief form, a generalized model of the photorefractive medium, which includes a dynamical equation for the pump wave (the one which creates the lattice). In the latter case, we demonstrate that, in the lowest nontrivial approximation, the probe field *does not* give rise to a feedback perturbing the lattice. In the rest of the paper, we chiefly focus on the study of the properties of gap solitons in our CMT models, as these models are subjects of interest in their own right, representing a new class of couple-mode equations. In Sec. III, we find analytical solutions for GS's in the 1D model and construct a full family of gap solitons in a numerical form for both models. In the same section, we report results which make it possible to identify stability regions of the GS's (which are quite different in the 1D and Q1D models, as two disjointed stability intervals are found in the latter one). In Sec. IV, tilted ("moving") gap solitons are considered, and their stability border is identified (we find that it does not depend on the tilt). The existence of stable tilted solitons in the *full model* of the photorefractive medium with the embedded photonic lattice is shown too. To the best of our knowledge, this is *the first demonstration* of stable tilted solitons in this physically important model. In Sec. IV, we also consider collisions between tilted solitons, which may be both elastic and inelastic. The paper is concluded by Sec. V.

II. COUPLE-MODE EQUATIONS

Following Refs. [3–5], we consider the propagation of a probe beam with the extraordinary polarization through a periodic structure in an (effectively planar) photorefractive medium. The structure is written by counterpropagating pump beams launched in the ordinary polarization. The electro-optic coefficients in the crystal strongly differ for the two polarizations, the waves in the ordinary polarization being nearly linear. Therefore, the optically induced grating, which is created, in the x direction, by the interference pattern of the counterpropagating beams, is essentially harmonic, with the intensity distribution $I_g(x)=I_0\cos^2(Kx)$, where

$$K = 2\pi n_0 \lambda^{-1} \cos\theta, \tag{1}$$

λ is the pump wavelength, θ is the angle between wave vectors of the plane waves and the x axis, and n_0 is the refractive index in the ordinary polarization. Provided that the intensity of the probe beam, $|E|^2$, is much weaker than the pump intensity I_0, one may neglect feedback action of the probe beam on the grating (this point will be substantiated below). Then the evolution of the local amplitude $E(x,z)$ of the probe beam in the free direction z obeys a known equation [3–5], whose normalized form is

$$i\frac{\partial E}{\partial z} + \frac{1}{2}\frac{\partial^2 E}{\partial x^2} - \frac{E}{1 + I_0\cos^2(Kx) + |E|^2} = 0. \tag{2}$$

A. One-dimensional model

To derive the coupled-mode equations for the forward and backward waves, we approximate solutions of Eq. (2) by

$$E(x,z) = u(x,z)e^{iKx} + v(x,z)e^{-iKx}, \tag{3}$$

where u and v are slowly varying [in comparison with the carrier waves $\exp(\pm iKx)$] envelopes of the forward and backward waves. Substituting the expansion (3) into Eq. (2), we perform the Fourier expansion with respect to $\exp(\pm iKx)$ and, in the spirit of the CMT approach, keep only the lowest-order harmonics. After a straightforward calculation, this leads to the following equations:

$$i\frac{\partial u}{\partial z} + iK\frac{\partial u}{\partial x} = \frac{(u-v)}{\sqrt{I_0(1+|u-v|^2)+1+2(|u|^2+|v|^2)}},$$

$$i\frac{\partial v}{\partial z} - iK\frac{\partial v}{\partial x} = \frac{(v-u)}{\sqrt{I_0(1+|u-v|^2)+1+2(|u|^2+|v|^2)}}. \tag{4}$$

Equations (4) constitute a *CMT model* with saturable nonlinearity. It contains one irreducible parameter I_0, while K may be absorbed into rescaling of x. Note that the expansion of the saturable nonlinearity in these equations up to the $\chi^{(3)}$ (cubic) order generates not only XPM and SPM terms, as in the usual generalized massive Thirring model, but also FWM (four-wave-mixing) ones, u^2v^* and v^2u^*, which originate from the terms $|u-v|^2u$ and $|u-v|^2v$ in the two equations.

Equations (4) can be combined into a system in which one equation is linear,

$$i\frac{\partial}{\partial z}(u-v) + iK\frac{\partial}{\partial x}(u+v) \tag{5}$$

$$-\frac{2(u-v)}{\sqrt{I_0(1+|u-v|^2)+1+2(|u|^2+|v|^2)}} = 0, \tag{6}$$

$$i\frac{\partial}{\partial z}(u+v) + iK\frac{\partial}{\partial x}(u-v) = 0. \tag{7}$$

In the physically relevant case, the photonic-lattice intensity is large—i.e., $I_0 \gg 1, |u|^2, |v|^2$; hence, the square root in Eq. (6) may be approximated by $\sqrt{I_0(1+|u-v|^2)}$, except for a vicinity of point(s) where $w \equiv u-v$ vanishes. Using this approximation and eliminating $(u+v)$ by means of Eq. (7), we reduce Eq. (6) to a single equation for $w(z,x)$,

$$\frac{\partial^2 w}{\partial z^2} - K^2\frac{\partial^2 w}{\partial x^2} + \frac{2i}{\sqrt{I_0}}\frac{\partial}{\partial z}\left(\frac{w}{\sqrt{(1+|w|^2)}}\right) = 0. \tag{8}$$

We have checked the accuracy of the simplified equation (8), comparing its analytical solutions for solitons (see below) and their stability with direct numerical solutions of Eqs. (6) and (7). As will be shown in Sec. III, a conspicuous difference appears only in the region of $I_0 \lesssim 3$, where the CMT does not adequately approximate Eq. (2) anyway.

Linearization of Eq. (8) and substitution of linear-wave solutions in the form of $w \sim \exp(iqz+ipx)$ yields the dispersion relation $\sqrt{I_0}q = -1 \pm \sqrt{1+I_0K^2p^2}$, according to which the band gap which may host GS's is

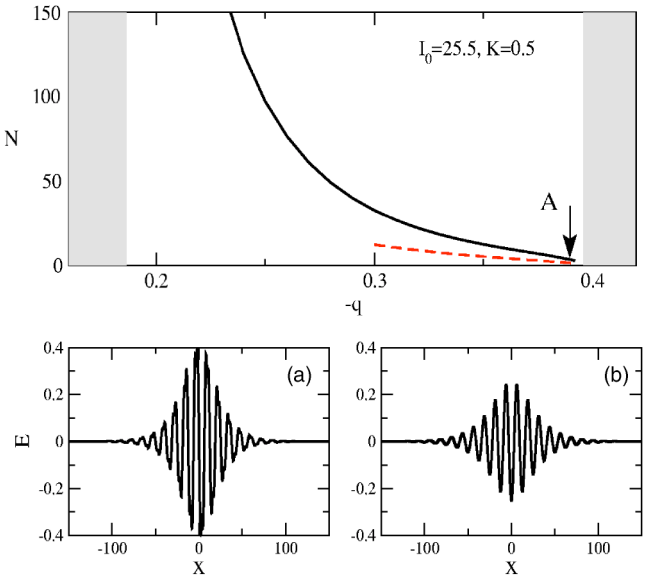

FIG. 1. The integral power of the soliton vs the propagation constant, in the first finite band gap of Eq. (2) (the shaded areas are the Bloch bands which confine the band gap). The parameters are $I_0=25.5$ and $K=0.5$. The solid and dashed lines show, respectively, a direct numerical solution of the stationary version of Eq. (2) and the analytical one, as obtained from Eqs. (18), (17), and (3). Examples of numerical (a) and analytical (b) profiles of the soliton, taken close to the edge of the band gap (at $q=0.39$, point A), are shown in the bottom part of the figure.

$$0 < -q < 2/\sqrt{I_0} \equiv Q \tag{9}$$

[without the above simplification which led to Eq. (8), the linearization of Eqs. (4) yields the band gap which differs from Eq. (9) by the substitution $I_0 \to I_0+1$]. In comparison with the first exact finite gap in the underlying equation (2), where we will compare the solitons found from Eqs. (2) and (4) for large I_0 (see Fig. 1 below), the band gap (9) is broader, roughly, by a factor $\simeq 1.6$.

B. Quasi-one-dimensional model

Another physically relevant possibility is to consider a two-dimensional (actually, Q1D) situation, with the angle between the wave vectors $\mathbf{k}_{1,2}$ of the probe waves and the axis z essentially different from 90°, while the spatial evolution is still in the direction of z (cf. a similar configuration, but for a model with quadratic nonlinearity, introduced in Ref. [20]). In this case, the difference from the above derivation formally amounts to the fact that, in the expression $|u-v|^2 \equiv |u|^2+|v|^2-(uv^*+u^*v)$, the wave-mixing terms (the last two ones) must be dropped, as they correspond to the combinations $\pm(\mathbf{k}_1-\mathbf{k}_2)$ of the wave vectors, which, if later added to the basic wave vectors $\mathbf{k}_{1,2}$, generate new ones, $2\mathbf{k}_{1,2}+\mathbf{k}_{2,1}$. In the 1D model proper, with $\mathbf{k}_2=-\mathbf{k}_1$, one has $2\mathbf{k}_{1,2}+\mathbf{k}_{2,1} \equiv \mathbf{k}_{1,2}$; hence, the wave-mixing terms contribute to the coupled-mode equations that are derived by dropping all the harmonics but the two basic ones. However, in the Q1D situation, the wave vectors $2\mathbf{k}_{1,2}+\mathbf{k}_{2,1}$ generate different harmonics. Thus, with regard to the underlying assumption $I_0 \gg 1$, the Q1D version of the CMT equations takes the form

$$i\frac{\partial u}{\partial z} + iK\frac{\partial u}{\partial x} = \frac{(u-v)}{\sqrt{I_0(1+|u|^2+|v|^2)}},$$

$$i\frac{\partial v}{\partial z} - iK\frac{\partial v}{\partial x} = \frac{(v-u)}{\sqrt{I_0(1+|u|^2+|v|^2)}}; \tag{10}$$

cf. Eqs. (4). Note that the band gap generated by the linearized version of these equations coincides with Eq. (9). As well as in the case of the 1D version proper, Eqs. (10) can be combined into the linear equation (7), but the remaining nonlinear equation cannot be reduced to a relatively simple equation for the single function w, unlike Eq. (6).

C. Feedback of the probe waves onto the photonic lattice

To conclude the consideration of the models, it is relevant to briefly address the issue of the reciprocal effect of the probe waves in the extraordinary polarization on the pump waves, which form the photonic lattice in the ordinary polarization. To this end, we assume that the strong field F which builds the grating and the weaker signal field E obey a system of coupled equations

$$\hat{L}F - \frac{F}{1+|F|^2+|E|^2} = 0, \tag{11}$$

$$iE_z + \frac{1}{2}\nabla^2 E - \frac{F}{1+|F|^2+|E|^2} = 0; \tag{12}$$

cf. Eq. (2). Here, $\hat{L}$ is a linear operator governing the propagation of the strong field (its exact form is not essential; see below) whose eigenmode $F_k^{(0)}$, which gives rise to the grating, is such that

$$|F_k^{(0)}|^2 = I_0 \cos^2(kx), \tag{13}$$

as was assumed above. The only essential conjecture about Eqs. (11) and (12) is that the interaction terms in both equations are derived from the *single term* in the system's Lagrangian density, which is $\mathcal{L}_{\rm int}=-\ln(1+|F|^2+|E|^2)$.

As before, we assume a signal field in the form of Eq. (3). Now, we also assume that the feedback from the E field will affect the F field, so that the solution for the latter field should be looked for, instead of the "frozen" form (13), as

$$|F_k|^2 = I(z,x)\cos^2[kx+\phi(z,x)], \tag{14}$$

where I and ϕ are slowly varying functions. To take the feedback into regard, we substitute expressions (3) and (14) into Eqs. (12) and (11) and perform the calculation in the first nontrivial approximation with respect to the small parameter $I^{-1/2}$. In fact, for Eq. (12) this was done before, leading to Eqs. (4). In the proper-1D model, the approximation leads to a Fourier expansion in the form

$$\frac{1}{1+|F|^2+|E|^2} = \frac{1-2\cos(2kx+2\phi)}{\sqrt{I}\sqrt{1+|u-v|^2}} + \text{h.o.h.}, \tag{15}$$

where "h.o.h." stands for higher-order harmonic terms. After the substitution of this in Eq. (11) and taking into regard that

the strong field F is carried by the harmonic $\cos(kx+\phi)$ [see Eq. (14)], we conclude that, in the present approximation, source terms that would drive slow evolution of $I(z,x)$ and $\phi(z,x)$ *cancel out to be zero*. This result actually amounts to an elementary fact: the expression $\cos(kx+\phi)[1-2\cos(2kx+2\phi)]\equiv-\cos(3kx+3\phi)$ does not contain a term $\sim\cos(kx+\phi)$.

With straightforward modifications, the same result can be obtained for the Q1D model. Thus, for both models considered here, the conjecture of the frozen lattice field, which was tacitly adopted above, is definitely justified for the large background intensity I_0.

III. STATIONARY GAP SOLITONS

A. One-dimensional model

Proceeding to soliton solutions of the CMT systems introduced above, we start with the simplified version of the 1D model, Eq. (8). The solution is sought for as $w(x,z)=e^{iqz}W(x)$, where q is a real propagation constant and a real function W obeys the equation $d^2W/dx^2=-d\Pi_{\rm eff}/dW$, with an effective potential

$$\Pi_{\rm eff}(W)=\frac{q^2}{2K^2}W^2+\frac{2q}{K^2\sqrt{I_0}}(\sqrt{1+W^2}-1). \tag{16}$$

Equation (7) shows that, for the stationary solutions, the underlying fields u and v can be expressed in terms of $W(x)$,

$$\{u,v\}=\frac{1}{2}e^{i(qz+\phi_0)}\left(\frac{iK}{q}\frac{dW}{dx}\pm W\right), \tag{17}$$

where ϕ_0 is an arbitrary phase shift.

It is easy to check that, if the propagation constant q belongs to the interval (9), the effective potential (16) has two symmetric minima, giving rise to GS solutions that can be written in an implicit analytical form,

$$K^2\left(\frac{dW}{dx}\right)^2=-(qW)^2+\frac{4|q|}{\sqrt{I_0}}(\sqrt{1+W^2}-1). \tag{18}$$

As follows from Eq. (18), the squared amplitude of the soliton's wave field, which is attained at a point where dW/dx vanishes, is

$$W_{\rm max}^2=\frac{8}{q^2I_0}(2-\sqrt{I_0}|q|).$$

In the small-amplitude limit—i.e., for

$$0<\epsilon\equiv 2(2-|q|\sqrt{I_0})\ll 1 \tag{19}$$

[which implies proximity to the right edge of the band gap (9)]—the GS asymptotically coincides with the conventional nonlinear-Schrödinger soliton,

$$W(x)=\sqrt{\epsilon}\,\mathrm{sech}\left(\sqrt{\frac{\epsilon|q|}{2}}\frac{x}{KI_0^{1/4}}\right). \tag{20}$$

Note that, in this case, expressions (17) can be cast in a closed form,

$$\{u,v\}\approx\pm\frac{\sqrt{\epsilon}}{2}e^{iqz}\,\mathrm{sech}\left(\sqrt{\frac{\epsilon|q|}{2}}\frac{x\pm iK/q}{KI_0^{1/4}}\right), \tag{21}$$

which mimics the exact form of the GS solution in the generalized massive Thirring model [16]; however, in the present model it is only an approximation valid for small ϵ.

In the other limit, $|q|\to 0$ [close to the left edge of the band gap (9)], the soliton assumes the shape of a broad "compacton" with a large amplitude,

$$W(x)=\frac{4}{|q|\sqrt{I_0}}\cos^2\left(\frac{|q|x}{KI_0^{1/4}}\right),\quad \text{if } |x|<\frac{\pi KI_0^{1/4}}{2|q|}, \tag{22}$$

and $W(x)=0$, if $|x|>\pi KI_0^{1/4}/(2|q|)$. However, the conditions under which Eqs. (4) were derived from Eq. (2) do not hold in the latter case, and as will be shown below, the compacton belongs to an unstable part of the soliton family.

To verify the validity of the CMT approximation for the description of solitons in the underlying photorefractive model (2), in Fig. 1 we compare the family of analytical solutions based on Eq. (18) and the ones found numerically from Eq. (2). The comparison is presented in terms of a global characteristic of the soliton family—viz., the integral power, $N=\int_{-\infty}^{+\infty}|E(x)|^2dx$—vs the propagation constant q. The approximation (3), which assumes that the amplitudes u and v are slowly varying functions of x in comparison with $\exp(\pm iKx)$, yields the integral power in terms of the CMT description:

$$N=\int_{-\infty}^{+\infty}(|u|^2+|v|^2)dx. \tag{23}$$

An example of direct comparison of the soliton's shapes is also included in Fig. 1. Naturally, the approximation is appropriate sufficiently close to the band gap's edge, when both models yield broad solitons. We also note that the negative slope of the $N(q)$ curve suggests stability of the entire soliton family as per the VK criterion—i.e., the absence of real eigenvalues in the spectrum of small perturbations around the soliton [19]. However, the solitons may be subject to oscillatory instabilities corresponding to complex eigenvalues; see below.

Although Fig. 1 shows that the direct applicability of the CMT approximation is limited to a rather narrow interval of values of the propagation constant q, we find it relevant to study the solitons generated by the two new CMT systems in a systematic way, as the topic is of interest in its own right, representing GS's of a new type. Results of the consideration are reported below.

Stationary solutions to the CMT equations (4) [without the simplification leading to Eq. (8)] were looked for as

$$\{u(z,x),v(z,x)\}=e^{iqz}\{U(x),V(x)\}, \tag{24}$$

applying the shooting method to the resulting equations for $U(x)$ and $V(x)$. A typical example of a stable GS found near the edge of the band gap (9) is displayed in Fig. 2 (the soliton stability is considered in detail below). It features the symmetry $U(-x)=-V(x)$, which is obviously compatible

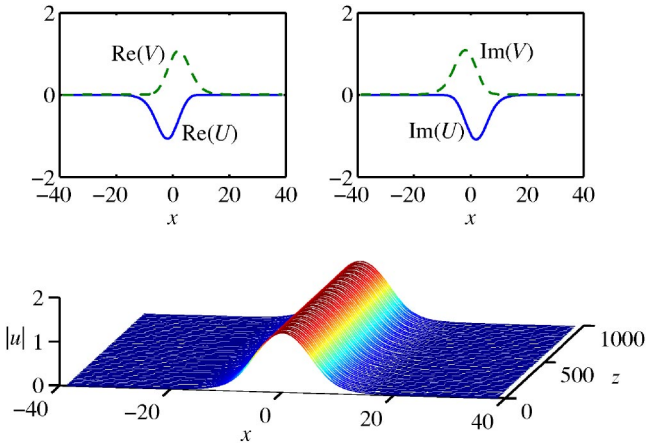

FIG. 2. A gap soliton found in the full CMT system (4), at the same values of the parameters, $I_0=25.5$ and $K=0.5$, which were used in Fig. 1. Here, $q=-0.2$ [cf. the value $Q\approx 0.4$ at the edge of the corresponding band gap (9)]. In fact, this soliton is quite accurately approximated by the analytical expressions (17) (with $\phi_0=-3\pi/4$) and (20). The lower panel illustrates the dynamical stability of the soliton.

with Eqs. (4) and is the same as in the generalized massive Thirring system.

Global characteristics of the soliton families are shown, in terms of the $N(q)$ dependence, in Fig. 3. This figure, which shows the soliton families as found from both the CMT system (4) and its simplified version (8), in which the solitons are available in the implicit analytical form (18), demonstrates that a tangible difference between the CMT model and its simplified version appears only at small values of I_0, for which, actually, the CMT equations cannot be derived from Eq. (2). We notice that all the $N(q)$ curves satisfy the VK criterion, $dN/dq<0$.

The stability of the GS's was tested by direct simulations, which used the filtered pseudospectral method in x, and the

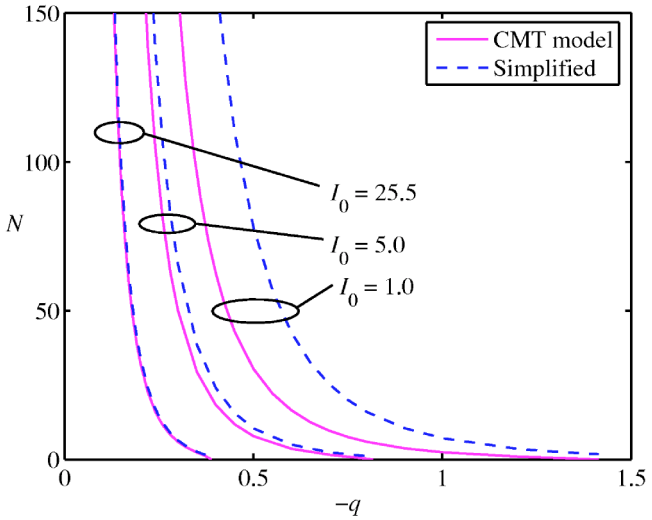

FIG. 3. The dependences $N(q)$ for the stationary solitons, found in a numerical form from the full system of the the 1D coupled-mode equations (4) and for the analytical solutions of the simplified system, which are given, in an implicit form, by Eqs. (18) and (17).

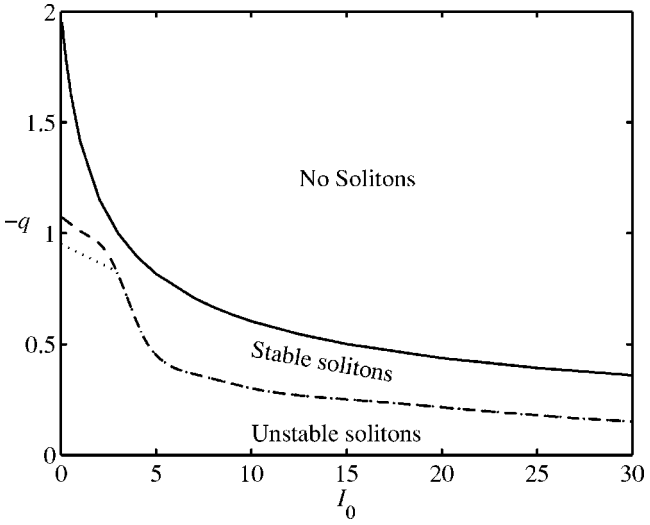

FIG. 4. The dashed and dotted lines are, respectively, stability borders of the gap solitons in the full coupled-mode system (4) and in its simplified version which amounts to Eq. (8). The upper solid border is the band gap's edge, $q=2/\sqrt{I_0}$; see Eq. (9).

fourth-order Runge-Kutta algorithm for advancing in z. As a result, an *intrinsic stability border*, which is shown in Fig. 4, was identified inside the GS family. When the GS's are unstable, their instability is only oscillatory, in accordance with the above findings showing that all the GS solutions are VK stable. An example of onset of the instability is shown in Fig. 5. Eventually, the unstable solitons get completely destroyed by the growing perturbations (rather than rearranging themselves into stable solitons).

We have also tested robustness of the GS's against diverse large perturbations. Generally, the stable solitons survive large disturbances; an example is shown in Fig. 6, where the soliton was perturbed by suddenly introducing a phase shift of $\approx 0.4\pi$ between its u and v components.

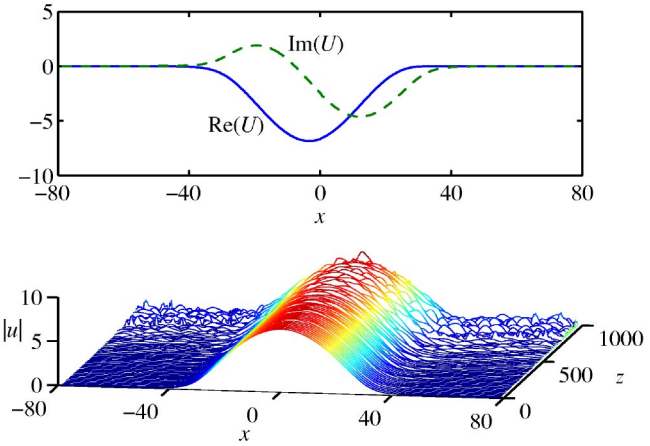

FIG. 5. The lower panel shows an example of the spontaneous onset of oscillatory instability in the u component of the gap soliton in the case of $I_0=25.5$, $K=0.5$, and $q=-0.05$ (the initial profile of the soliton is shown in the upper panel). The instability grows from a very small numerical noise. In this figure and below, the dynamics is shown only in the u component if the picture in the v component turns out to be very similar.

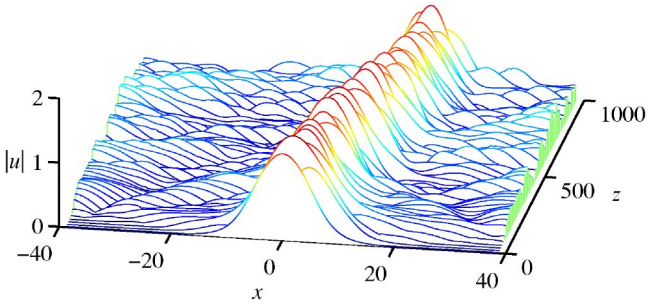

FIG. 6. A result of sudden multiplication of the u and v components of the stable soliton shown in Fig. 2 by phase-shifting factors $0.8\pm0.6i$. The parameters are $I_0=25.5$, $K=0.5$, and $q=-0.2$.

B. Quasi-one-dimensional model

Searching for stationary solutions to Eqs. (10) of the Q1D model in the form of Eq. (24), it is easy to derive a single equation for $W(x)\equiv U(x)-V(x)$:

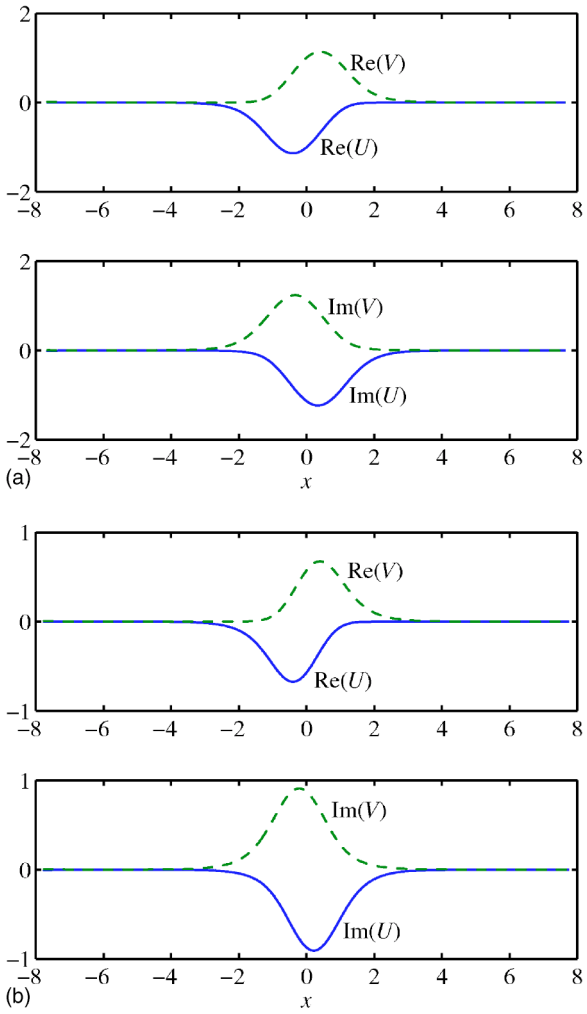

FIG. 7. Typical examples of stationary solitons found in the quasi-1D model based on Eqs. (10) and (24) with $K=0.5$ and $I_0=1$: (a) $q=-1.125$ and (b) $q=-1.4$.

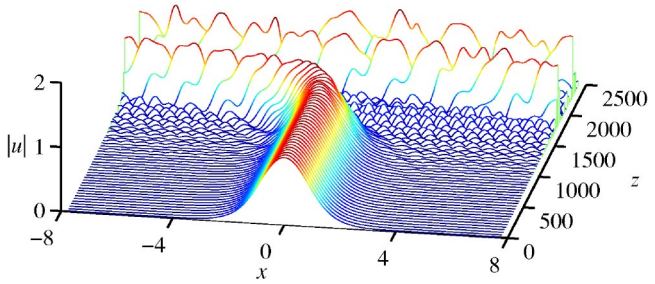

FIG. 8. Instability of the soliton in the quasi-1D model, whose stationary form is shown in Fig. 7(b).

$$\frac{d^2W}{dx^2}+\frac{q^2}{K^2}W+\frac{2q}{K^2\sqrt{I_0}}\frac{W}{\sqrt{1+W^2+(dW/dx)^2}}=0, \qquad (25)$$

the fields $U(x)$ and $V(x)$ being expressed in terms of W the same way as in Eq. (17). Equation (25) does not admit exact analytical solutions. However, close to the right edge of the gap (9)—i.e., when ϵ, defined as per Eq. (19), is small—an approximate solution takes the form of Eq. (20), with an additional factor of $\sqrt{2}$.

As mentioned above, both parameters K and I_0 can be scaled out from the Q1D model; therefore, to present further results, we will fix $K=0.5$ (as above) and $I_0\equiv1$. The band gap (which is $0<-q<2$, in the notation adopted here) is entirely filled with numerically found soliton solutions. Even not very close to the right edge of the gap, the solutions, whose typical examples are shown in Fig. 7, are quite similar to those found above in the proper-1D model; cf. Fig. 2. However, stability properties of the GS's in the Q1D model, which were inferred from direct numerical simulations, turn out to be very different in comparison with those reported above for the 1D model proper. Namely, Eqs. (10) generate *two disjointed* stability regions inside the band gap: a narrow one, $1.100<-q<1.125$, and a broader region, $1.6<-q<2$, which, as well as its counterpart in the proper-1D model, abuts on the right edge of the band gap (note, however, that

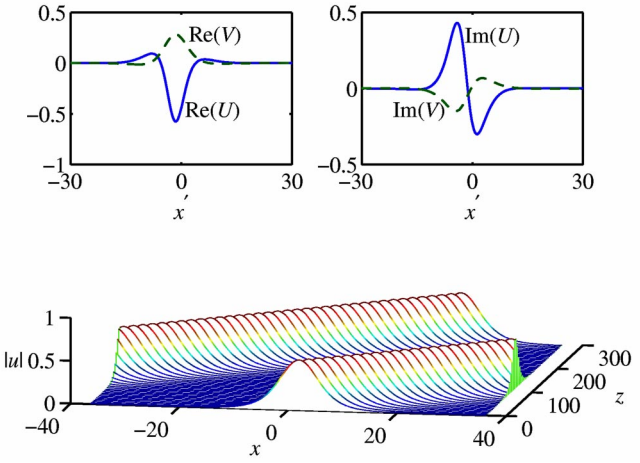

FIG. 9. A typical example of a stable tilted soliton in the 1D model (4), found for $K=0.5$ and $I_0=25.5$. The soliton corresponds to $q=-0.3$ and $c=0.3$ in Eq. (26).

the relative width of this region, in comparison with the entire band gap, is much smaller than in the proper-1D model; cf. Fig. 4). In particular, the soliton shown in Fig. 7(a), which is located just at the edge of the narrower stability region, is completely stable, while the one shown in Fig. 7(b) is unstable, as illustrated by Fig. 8.

IV. TILTED GAP SOLITONS

A. Coupled-mode equations

The CMT approximation opens a way to investigate novel phenomena which may be difficult to study directly within the framework of the underlying models. An issue of obvious interest are tilted (moving) GS's, of the form $(u,v)=e^{iqz}(U(x-cz),V(x-cz))$. We will consider them only for the 1D model based on Eqs. (4); however, results for tilted solitons in the Q1D model (10) are quite similar.

Straightforward analysis, in the coordinate system $(z,x-cz)$ [instead of the original system (z,x)], shows that, if the solutions are sought for as

$$\{u,v\}=e^{iqz}\{U(x'),V(x')\},\quad x'\equiv x-cz \tag{26}$$

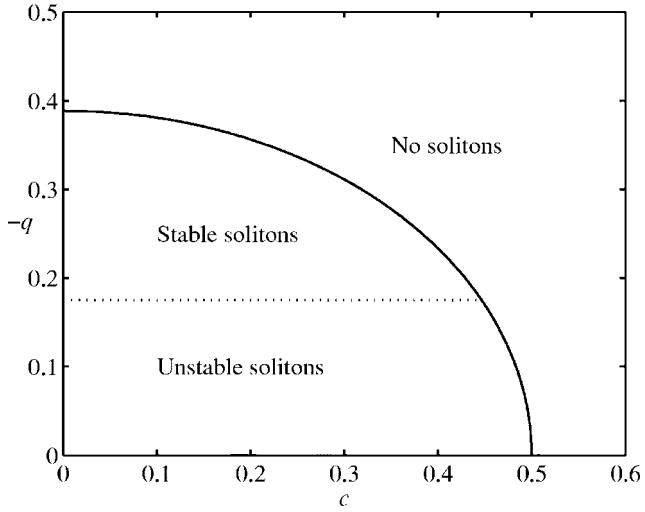

FIG. 10. The stability region for titlted solitons in the proper-1D model with $K=0.5$ and $I_0=25.5$. Up to the accuracy of the numerical results, the border does not depend on the tilt c.

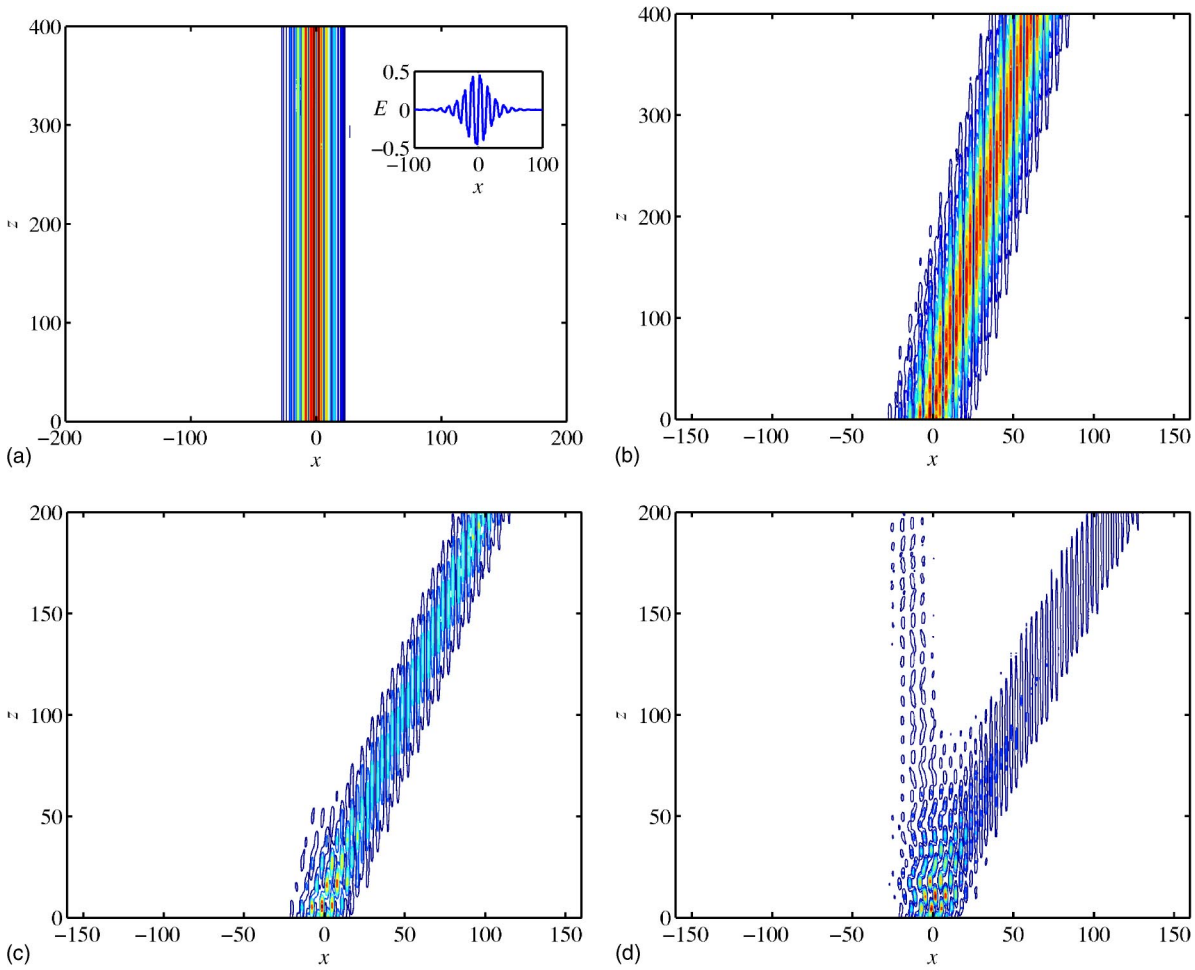

FIG. 11. The application of the initial shove, in the form of the multiplication by $\exp(ikx)$, to a stationary soliton in the underlying equation (2) with $K=0.5$ and $I_0=25.5$. The results are presented by dint of contour plots of the local power, $|u(z,x)|^2+|v(z,x)|^2$. The initial stable soliton, taken with $q=-0.388$, is shown in (a) (with its profile in the inset). The shove with $k=0.05$ (b) and $k=0.2$ (c) generates stable titled solitons, after some loss; the shove with $k=0.4$ (d) destroys the soliton.

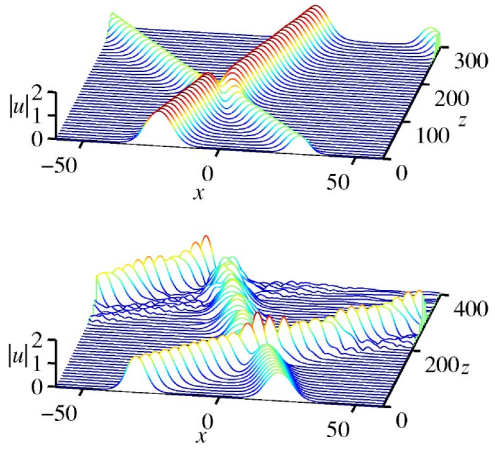

FIG. 12. Typical examples of elastic and inelastic collisions between titled solitons in the 1D model (4). In this case, $I_0=25.5$, $K=0.5$, both solitons have $q=-0.2$, and their velocities are $c_1=0.3$, $c_2=-0.1$. The difference is that, in the case of the elastic collision (upper panel), the phase difference between the solitons is $\Delta\phi=\pi$, while in the case of the inelastic collision, $\Delta\phi=0$.

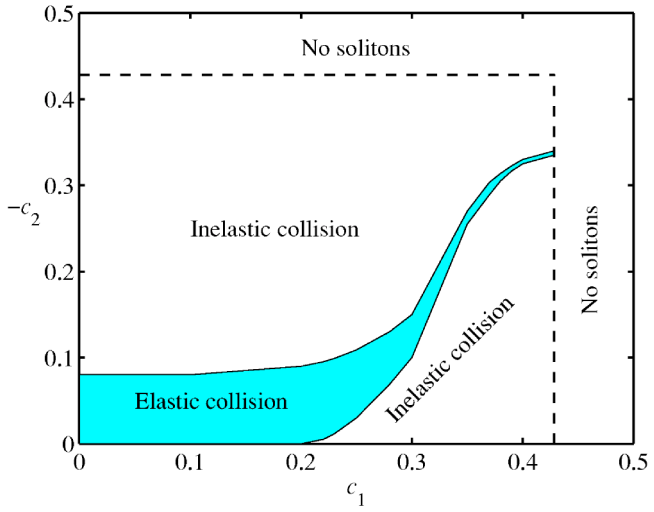

FIG. 13. Regions of elastic and inelastic head-on collisions between two solitons, with tilts $c_1>0$ and $c_2<0$, and $q_1=q_2=-0.2$ (close to the instability border, which is at $q\approx-0.19$, in this case), in the 1D model (4) with $I_0=25.5$ and $K=0.5$.

[cf. Eq. (24)], the band gap (9) shrinks to

$$0<-q<Q'\equiv Q\sqrt{1-(c/K)^2}, \tag{27}$$

and it does not exist for $|c|>c_{\max}^{(\mathrm{CMT})}\equiv K$.

Numerical solution of equations obtained by the substitution of the ansatz (26) into Eqs. (4) demonstrates that the reduced gap (27) is completely filled with tilted GS's. An example of a stable tilted soliton is shown in Fig. 9.

The stability of the tilted solitons was also tested in direct simulations. As a result, it has been found that, up to the available numerical accuracy, the stability border (i.e., the value q_{cr} separating stable and unstable solitons) does not depend on the tilt ("velocity") c. An example of this is shown in Fig. 10. Following the pattern of this figure, the stability region in the $(c,-q)$ plane for any fixed I_0 can be identified by simply drawing the horizontal line at the value $q=q_{\mathrm{cr}}$ taken, for the same I_0, from Fig. 4. The fact that the stability border does not depend on c resembles a known feature of the GS family in the conventional generalized massive Thirring model, where the dependence of the stability border on the soliton's velocity is extremely weak [18].

B. Tilted solitons in the full photonic-lattice model

The existence of tilted solitons in the CMT system suggests that they may also be found in the underlying equation (2), which is the model of the photorefractive medium with the induced photonic lattice. To check this possibility, we simulated Eq. (2), multiplying numerically exact untilted solitons by $\exp(ikx)$, in order to "shove" them. Gradually increasing k, we observed an increase of the tilt c in the resulting stable soliton, up to some value $c_{\max}$ at $k=k_{\max}$, beyond which the soliton was destroyed by the shove. An example of this sequence of results, together with the original soliton, is shown in Fig. 11. Note that the maximum tilt $c_{\max}$ achievable in the simulations of Eq. (2) in this example is quite close to 0.5; on the other hand, Eq. (27) shows that, within the framework of the CMT system, $c_{\max}^{(\mathrm{CMT})}=K=0.5$. The latter demonstrates that (for I_0 sufficiently large) the CMT approximation provides good accuracy for the tilted solitons as well.

C. Soliton collisions

The stability of the tilted solitons suggests a possibility to consider collisions (intersections) between them. The most important characteristic of soliton collisions is elasticity. Direct simulations of the 1D model (4) demonstrate that the interaction between the solitons is quite elastic, unless they are taken close to the instability border (the border is shown in Fig. 10). Examples of elastic and inelastic collisions are displayed in Fig. 12. Note that, in this example, the two cases are identical, except for the phase difference $\Delta\phi$ between the solitons. In the case of the elastic collision, they have $\Delta\phi=\pi$; hence, they repel each other, thus avoid strong overlapping, which explains the elastic character of the collision. In the opposite case, they have $\Delta\phi=0$ and therefore attract each other. As a result, they strongly overlap during the collision (actually passing through each other), thus generating strong mutual disturbances. However, it should be stressed that, even in the case of the inelastic collision, neither soliton gets completely destroyed (not only in this example, but also in the generic case).

Note that proximity of the solitons to the stability border is determined by their propagation constants $q_{1,2}$, but not the initial tilts $c_{1,2}$, as the stability border does not depend on c. However, the elasticity of the collision strongly depends, in this case, on c_1 and c_2, as shown in Fig. 13. The form of the elasticity region displayed in this figure is quite typical for a soliton pair taken close to the instability border. The lack of symmetry relative to the diagonal, $c_1=-c_2$, is due to the fact that, below and above the diagonal, the colliding solitons were taken, respectively, with $\Delta\phi=\pi$ and $\Delta\phi=\pi$, similar to the two different cases displayed in Fig. 12.

V. CONCLUSIONS

In this paper, we have derived two forms of the coupled-mode theory for spatial gap solitons in photonic lattices optically written in a photorefractive medium. One model pertains to the 1D case proper and the other one to the Q1D case. The models differ substantially from the ordinary coupled-mode system (the generalized massive Thirring model) by a saturable character of the nonlinearity and the presence of FWM terms if the nonlinearity is expanded up to cubic order. Besides the application to photorefractive media, these models represent a novel type of CMT systems; therefore, they are of considerable interest by themselves. Stationary solitons in the 1D model have been found in an implicit analytical form, and in the Q1D model they have been found numerically. Stability of the solitons has been tested by means of direct numerical simulations, revealing a nontrivial intrinsic border of instability against oscillatory perturbations. In the Q1D model, two disjointed stability regions have been found.

The soliton family has been extended to include tilted (moving) solitons. Their stability region has been identified too, with the conclusion that the stability border does not depend on the tilt. Stable tilted solitons have also been found in direct simulations of the full model of the photonic lattice in the photorefractive medium. The CMT correctly predicts the maximum tilt up to which the stable solitons can be found in the full model. As far as we know, this is the first demonstration of the existence of stable tilted solitons in the model of the photorefractive crystal with the embedded photonic lattice.

Collisions between tilted solitons have been investigated too, showing that they are chiefly elastic, except close to the instability border. In the latter case, the elastic or inelastic character of the collision also depends on the phase shift between the solitons. The theoretical results reported in this work suggest new experiments with spatial solitons in optically induced lattices in photorefractive media.

ACKNOWLEDGMENTS

B.A.M. appreciates hospitality of the Nonlinear Physics Center at the Australian National University. His work was supported, in part, by the Israel Science Foundation through Grant No. 8006/03. B.A.M. and T.M. are indebted to the Optoelectronics Research Center at the City University of Hong Kong, where a part of the work was carried out. Y.S.K. is a member of the Centre for Ultra-high bandwidth Devices for Optical Systems (CUDOS) of the Australian Research Council.

[1] *Nonlinear Photonic Crystals*, edited by R. E. Slusher and B. J. Eggleton, Springer Series in Photonics, Vol. 10 (Springer-Verlag, Berlin, 2003).
[2] Yu. S. Kivshar and G. P. Agrawal, *Optical Solitons: From Fibers to Photonic Crystals* (Academic, San Diego, 2003).
[3] N. K. Efremidis, S. Sears, D. N. Christodoulides, J. W. Fleischer, and M. Segev, Phys. Rev. E **66**, 046602 (2002); N. K. Efremidis, J. Hudock, D. N. Christodoulides, J. W. Fleischer, O. Cohen, and M. Segev, Phys. Rev. Lett. **91**, 213906 (2003).
[4] J. W. Fleischer, T. Carmon, M. Segev, N. K. Efremidis, and D. N. Christodoulides, Phys. Rev. Lett. **90**, 023902 (2003).
[5] D. Neshev, E. A. Ostrovskaya, Yu. S. Kivshar, and W. Krolikowski, Opt. Lett. **28**, 710 (2003).
[6] J. W. Fleischer, M. Segev, N. K. Efremidis, and D. N. Christodoulides, Nature (London) **422**, 147 (2003); J. W. Fleischer, G. Bartal, O. Cohen, O. Manela, M. Segev, J. Hudock, and D. N. Christodoulides, Phys. Rev. Lett. **92**, 123904 (2004).
[7] C. M. de Sterke and J. E. Sipe, in *Progress in Optics*, edited by E. Wolf (North-Holland, Amsterdam, 1994), Vol. XXXIII, p. 203.
[8] B. J. Eggleton, R. R. Slusher, C. M. de Sterke, P. A. Krug, and J. E. Sipe, Phys. Rev. Lett. **76**, 1627 (1996).
[9] J. Feng, Opt. Lett. **18**, 1302 (1993).
[10] R. F. Nabiev, P. Yeh, and D. Botez, Opt. Lett. **18**, 1612 (1993).
[11] Yu. S. Kivshar, Phys. Rev. E **51**, 1613 (1995).
[12] W. C. K. Mak, B. A. Malomed, and P. L. Chu, Phys. Rev. E **58**, 6708 (1998).
[13] A. A. Sukhorukov and Yu. S. Kivshar, Opt. Lett. **27**, 2112 (2002).
[14] D. Mandelik, R. Morandotti, J. S. Aitchison, and Y. Silberberg, Phys. Rev. Lett. **92**, 093904 (2004); R. Morandotti, D. Mandelik, Y. Silberberg, J. S. Aitchison, M. Sorel, D. N. Christodoulides, A. A. Sukhorukov, and Y. S. Kivshar, Opt. Lett. **29**, 2890 (2004).
[15] D. Neshev, A. A. Sukhorukov, B. Hanna, W. Krolikowski, and Yu. S. Kivshar, Phys. Rev. Lett. **93**, 083905 (2004).
[16] A. B. Aceves and S. Wabnitz, Phys. Lett. A **141**, 37 (1989); D. N. Christodoulides and R. I. Joseph, Phys. Rev. Lett. **62**, 1746 (1989).
[17] B. A. Malomed and R. S. Tasgal, Phys. Rev. E **49**, 5787 (1994).
[18] I. V. Barashenkov, D. E. Pelinovsky, and E. V. Zemlyanaya, Phys. Rev. Lett. **80**, 5117 (1998).
[19] M. G. Vakhitov and A. A. Kolokolov, Radiophys. Quantum Electron. **16**, 783 (1973).
[20] W. C. K. Mak, B. A. Malomed, and P. L. Chu, Phys. Rev. E **58**, 6708 (1998).